4-19-2016

Novel Compound Heterozygous Mutations Expand the Recognized Phenotypes of *FARS2*-linked Disease

Melissa A. Walker
Massachusetts General Hospital

Kyle Mohler
The Ohio State University

Kyle W. Hopkins
The Ohio State University

Derek H. Oakley
Massachusetts General Hospital

David A. Sweetser
Massachusetts General Hospital

See next page for additional authors

Recommended Citation

Walker, M.A., Mohler, K.P., Hopkins, K.W., Oakley, D.H., Sweetser, D.A., Ibba, M., Frosch, M.P. and Thibert, R.L. (2016) Novel compound heterozygous mutations expand the recognized phenotypes of *FARS2*-linked disease. *J. Child Neurology* **31**, 1127-1137. https://doi.org10.1177/0883073816643402

Novel Compound Heterozygous Mutations Expand the Recognized Phenotypes of *FARS2*-linked Disease

Authors

Melissa A. Walker, Kyle Mohler, Kyle W. Hopkins, Derek H. Oakley, David A. Sweetser, Michael Ibba, Matthew P. Frosch, and Ronald L. Thibert

Published in final edited form as:

J Child Neurol. 2016 August ; 31(9): 1127–1137. doi:10.1177/0883073816643402.

Novel compound heterozygous mutations expand the recognized phenotypes of *FARS2*-linked disease

Melissa A. Walker, M.D., Ph.D.,
617-726-6093, 617-724-7860, 55 Fruit St., WACC 7th Floor, Department of Neurology, Division of Child Neurology, Massachusetts General Hospital, Boston, MA 02114

Kyle P. Mohler, B.S.,
Department of Microbiology, Ohio State University, Columbus, Ohio 43210

Kyle W. Hopkins, B.S.,
Department of Microbiology, Ohio State University, Columbus, Ohio 43210

Derek H. Oakley, M.D., Ph.D.,
Department of Pathology, Division of Neuropathology, Massachusetts General Hospital

David A. Sweetser,
Department of Medical Genetics, Massachusetts General Hospital, Boston, MA 02114

Michael Ibba,
Department of Microbiology, Ohio State University, Columbus, Ohio 43210

Matthew P. Frosch, and
Department of Pathology, Division of Neuropathology, Massachusetts General Hospital

Ronald L. Thibert
Department of Neurology, Division of Child Neurology, Massachusetts General Hospital, Boston, MA 02114

Melissa A. Walker: walker.melissa@mgh.harvard.edu; Kyle P. Mohler: mohler.69@buckeyemail.osu.edu; Kyle W. Hopkins: hopkins.693@buckeyemail.osu.edu; Derek H. Oakley: DOAKLEY@PARTNERS.ORG; David A. Sweetser: DSWEETSER@PARTNERS.ORG; Michael Ibba: ibba.1@osu.edu; Matthew P. Frosch: MFROSCH@PARTNERS.ORG; Ronald L. Thibert: rthibert@partners.org

Abstract

Mutations in mitochondrial aminoacyl-tRNA synthetases are an increasingly recognized cause of human diseases, often arising in individuals with compound heterozygous mutations and presenting with system-specific phenotypes, frequently neurologic. *FARS2* encodes mitochondrial phenylalanyl transfer RNA synthetase (mtPheRS), perturbations of which have been reported in 6 cases of an infantile, lethal disease with refractory epilepsy and progressive myoclonus.

Author Contributions: Melissa Walker, Kyle Mohler, Kyle Hopkins, and Michael Ibba drafted the manuscript, designed and conducted experiments. Melissa Walker, Derek Oakley, David Sweetser, Matthew Frosch, and Ronald Thibert provided interpretation of clinical studies. All authors provided revisions and editing of the manuscript.

Declaration of Competing Interest: The authors have no competing interests to declare.

Supplemental Data: Supplemental data include one figure.

Ethical Approval: No human or animal subjects used in experimentation.

Here we report the case of juvenile onset refractory epilepsy and progressive myoclonus with compound heterozygous *FARS2* mutations. We describe the clinical course over 6 years of care at our institution and diagnostic studies including electroencephalogram (EEG), brain magnetic resonance imaging (MRI), serum and cerebrospinal fluid analyses, skeletal muscle biopsy histology, and autopsy gross and histologic findings which include features shared with Alpers-Huttenlocher syndrome, Leigh syndrome, and a previously published case of *FARS2* mutation associated infantile onset disease. We additionally present structure-guided analysis of the relevant mutations based on published mitochondrial phenylalanyl transfer RNA synthetase and related protein crystal structures as well as biochemical analysis of the corresponding recombinant mutant proteins.

Keywords

FARS2; progressive myoclonus epilepsy; mitochondrial tRNA synthetase

Introduction

Defects in nuclear genes encoding mitochondrial aminoacyl-tRNA synthetases (mt-aaRS) are increasingly linked to a variety of pediatric and adult onset disorders[1], many with relative selectivity of organ systems affected, particularly the central nervous system[2, 3, 4, 5, 6]. The mechanism by which perturbations of aminoacyl-tRNA synthetases produce clinical phenotypes remains unclear, but is generally thought to involve a defect in mitochondrial translation, defects in other effects of which have been linked to other human diseases with similar phenotypes[7].

FARS2 (encoding mitochondrial phenylalanyl transfer RNA synthetase) is the nuclear encoded aminoacyl-tRNA synthetase required for the charging of the cognate mitochondrial tRNA with phenylalanine. Defects in this enzyme would presumably impact the expression of the 13 mitochondrially encoded peptides, including subunits of the mitochondrial respiratory chain[8]. To date, six individuals with *FARS2* mutations (3 siblings with homozygous missense mutations[11], 2 siblings with compound heterozygous missense mutations[10], and 1 infant with a missense mutation and a large deletion[9]) have been reported, all presenting with a clinical phenotype of infantile onset refractory epilepsy and myoclonus (Table 1)[9, 10, 11]. In all cases there was a characteristic, relative specificity of the phenotype to the central nervous system (CNS), all but one were deceased by age 3 – 24 months at the time of reporting. Of the 3 with MRI findings reported, all had abnormalities ranging from isolated white matter abnormalities[9] to cortical atrophy with putaminal signal abnormalities[10], and subdural fluid collections[11]. Decreased COX staining was reported in two patients[10, 11], but no ragged red fibers were observed in either of two patients with reported muscle biopsy[9, 10]. Serum lactate elevations were reported in three cases[9, 10]. In the sole individual for whom autopsy information was available, an Alpers-Huttenlocher-like features were reported including brain weight <30% of normal, generalized atrophy, gliosis, and subtotal laminar necrosis of the entire cortical ribbon[10]. The missense mutations reported in compound heterozygote and homozygote patients were all highly conserved in eukaryotic but not prokaryotic PheRS. One missense mutation from compound heterozygote

patients is located at the ATP-binding site while the other lies at an interdomain interface. The missense mutation of the homozygous patients maps to a distinct interdomain interface[10]. Recombinant mutant proteins for each of the missense mutations demonstrated decreased or mildly decreased catalytic efficiency and more severely impacted refolding compared to wild type in vitro[10].

Here, we report a case of a young woman with novel compound heterozygous *FARS2* mutations and a CNS-specific phenotype of childhood onset refractory epilepsy, progressive myoclonus with features in some brain regions reminiscent of Alpers-Huttenlocher syndrome and a previously published case of *FARS2* mutation associated infantile onset disease[10] as well as a region with findings similar to Leigh syndrome in addition to characterization of enzyme kinetics and apparent binding affinities of recombinant, mutant mtPheRs proteins.

Materials and Methods

Bioinformatics and structure-guided analysis

Multiple sequence alignments were performed using CLC Sequence Viewer Version 6.8.2 (CLC Bio, Qiagen). Crystal structures were reviewed and graphics created using Pymol12.

Functional assays

Protein Expression and Purification—*E. coli* Rosetta (DE3) cells containing pRARE plasmids encoding tRNAs for rare codons were transformed with either WT plasmid pET21c-PheRS (a gift from L. Spremulli, University of North Carolina, Chapel Hill, NC, USA) or mutant mtPheRS plasmids P85A and H135D. Point mutations were introduced by site directed mutagenesis using the QuickChange protocol (Stratagene). Cultures were grown at 37°C to OD = 0.8 and induced with 0.5 mM IPTG for 4 h. Cells were harvested, sonicated and supernatant was collected after centrifugation at 25 000×g for 1 h. The supernatant was applied to a TALON metal affinity resin column (Clontech), followed by washing and the protein was eluted with 25 mM Tris–HCl, pH 8.0, 300 mM NaCl, 250 mM imidazole and 10% glycerol. Fractions containing mtPheRS were checked for electrophoretic purity by SDS–PAGE, pooled and dialyzed overnight at 4°C in 50 mM Tris–HCl, pH 7.5, 5 mM MgCl2 and 100 mM KCl. The purified enzyme was concentrated, adjusted to 50% (v/v) glycerol and aliquots were stored at -80°C. *E. coli* $tRNA^{Phe}$ was made by T7 runoff transcription as previously described[13; 10]. DNA template for tRNA transcription was generated from plasmids carrying tRNA genes by PCR amplification. The tRNA was phenol chloroform extracted and purified on a DEAE sepharose column, as described previously[13, 10].

***In vitro* tRNA Aminoacylation—**Endpoint in vitro aminoacylation was performed at 37 °C in aminoacylation buffer [100mMNa-Hepes (pH 7.2), 30mMKCl, 2mM ATP, and 10 mM $MgCl_2$] containing 40 μM L-[^{14}C]Phe (174 cpm pmol–1; Perkin-Elmer Lifesciences), 5 μM E. coli $tRNA^{Phe}$ transcript, and 100 nM mtPheRS. 8 μl aliquots were removed and spotted on 3MM filter disks (Whatman), washed three times in 10% trichloroacetic acid, once with 95% ethanol, and then dried. The amount of radioactivity retained was determined

by liquid scintillation counting. Steady state kinetics for $tRNA^{Phe}$ were determined at 37 °C as described previously with concentrations of *in vitro* transcribed *E. coli* $tRNA^{Phe}$ varying between 0.1 and 5 μM and enzyme added to a final concentration of 100 nM[13].

ATP-PPi Exchange—ATP-PPi exchange rate for amino acid activation was determined according to standard methods as previously described[13]. Reactions were carried out at 37 °C in a medium containing 100 mM Na-Hepes (pH 7.2), 30 mM KCl, 10 mM $MgCl_2$, 2 mM NaF, 2 mM ATP, 2 mM [^{32}P]PPi (2 cpm/pmol), Phe (15 μM), and 50 nM mtPheRS. After 1–5 min, 25 μl of the reaction were removed and added to a solution containing 1% charcoal, 5.6% HClO4, and 75 mM PPi. The charcoal-bound ATP was filtered through a 3 MM Whatman filter discs under vacuum and washed three times with 5 ml of water and once with 5 ml of ethanol. The filters were dried, and the radioactivity content was determined by liquid scintillation counting.

Thermostability Assa—To assay protein stability, active fractions of 5 μM of all the protein samples were incubated at 37 °C. Enzyme activity was monitored by active-site titration and was performed in 50-μL reaction mixtures containing 100 mM Na-Hepes (pH 7.2), 30 mM KCl, 10 mM $MgCl_2$, 2 mM ATP, 40 μM L-[^{14}C]Phe (174 cpm pmol–1). Pyrophosphatase was also added to ensure a unidirectional formation of aminoacyl adenylate. The reaction was initiated by the addition of mtPheRS to a reaction mixture preincubated at 37 °C for 5 min. After addition of the enzyme, the reaction was performed for 10 min at 37 °C and then filtered through a nitrocellulose membrane (PROTRAN BA85; Whatman) prewashed with cold 0.5× aminoacylation buffer. The filters were then washed with 3 mL of cold 0.5× aminoacylation buffer and dried at 80 °C for 15 min. The amount of radioactivity retained was quantified by liquid scintillation counting.

Patient studies

Transient elevations of serum lactate were noted as high as 6.4mmol/L (normal range 0.5-2.2 mmol/L). Muscle biopsy included examination of skeletal muscle of the right thigh using hematoxylin and eosin stain, modified Gomori's trichrome, NADH reductase, oil red O, PAS, COX/SDH and ATPase (at pH 4.3, 4.6, and 9.4) stains as well as electron microscopy by standard methods. Microscopic analysis of formalin-fixed brain tissue was performed using hematoxylin, eosin, and luxol blue stains per standard methods.

Spectrophotometeric analysis of oxidative phosphorylation, skin fibroblast pyruvate dehydrogenase and pyruvate carboxylase activity, and butyrobetaine levels were performed at the Center for Inherited Disorders of Energy Metabolism (CIDEM, Case Western Reserve University). Assessment of mitochondrial DNA content of skeletal muscle was performed by qPCR analysis at Baylor University.

Results

Genetic findings

Dual genome panel by massively parallel sequencing (Baylor College of Medicine – MitomeNGS) revealed three nuclear variants of unknown significance and two

mitochondrial variants of unknown significance. Nuclear variants included two mutations in *FARS2*: c.253C>G (p.P85A, exon 2) and c.403C>G (p.H135D, exon2) as well as a single missense mutation in the pyruvate carboxylase gene *PC*, c.2786C>G (p.A929G, exon 20). The *PC* variant was predicted to be benign due to only moderate evolutionary conservation of Alanine-929 and inconsistency with the above reported clinical phenotype. A whole exome sequencing study was also performed (GeneDx, Gaithersburg, MD) that confirmed the two variants in the *FARS2* gene, and demonstrated compound heterozygosity, with one allele inherited from each parent. No other significant findings were found by whole exome sequencing.

Bioinformatics and structure-guided analysis

To better understand potential biologic implications of the *FARS2* mutations identified, bioinformatics and crystal structure-guided analysis were undertaken. Multiple sequence alignments of orthologous enzymes from mouse, chicken, amphibian, insect, yeast, and bacterial species were performed and reveal that the residues affected by the missense mutations are highly conserved through evolution, including in *Escherichia coli* (figure 1). Notably, the mutations identified each convert the amino acid in question to a residue with distinct biochemical properties. Proline-85, the residue with the most restrictive main chain conformations, is mutated to an alanine with both a greater number of potential main chain conformations and a more positive hydropathy score[14]. Likewise, histidine-135 is mutated to an aspartate, producing a complete charge reversal of the side chain. Review of the published crystal structure of the mtPheRS-Phe-AMP complex[15] identifies proline-85 as a buried residue while the side chain of histidine-135 is exposed. Both residues lie within the larger “catalytic domain,” though neither contacts the Phe-AMP moiety within the active site (figure 2a, 4b). Proline-85 constitutes the N-terminal most residue of the “Motif 1” alpha helix that, interestingly, is required for oligomerization of class II aminoacyl-tRNA synthetases and is speculated to perform other functions as well, though its significance in mtPheRs, which functions as a monomer is unclear. Histidine-135 forms part of an alpha helix within the region connecting Motif 1 and Motif 2, the second of three highly conserved structural elements common to class II aaRSs. In the crystal structure of the orthologous protein *T. thermophilus-PheRS-bound* to $tRNA^{Phe}$, this conserved inter-motif region forms one of two catalytic domain loops that associate with the acceptor stem of the tRNA molecule[16] (figure 2c). Of note, the *T. thermophilus* enzyme is a class II enzyme that like class I enzymes charges the 2′OH group (as opposed to the 3′-OH group) of the terminal tRNA ribose and is composed of two alpha-beta subunit heterodimers, in contrast to human mtPheRs which is monomeric but shares significant sequence homology with the alpha subunit of *T. thermophilus* PheRS.

Functional assays

To assess the impact of the identified P85A and H135D substitutions on enzyme function, we expressed and purified recombinant mutant mtPheRS proteins in *E. coli* per established protocols[13]. End point aminoacylation reactions indicated that P85A mtPheRS charges tRNA very similarly to WT, but H135D demonstrated severe aminoacylation deficiency (figure 3). Determination of the steady-state kinetics for tRNA revealed that mutant P85A has a two-fold increase in catalytic efficiency when compared to WT, while kinetic

parameters for H135D were unable to be determined using standard techniques, reinforcing the previously observed aminoacylation deficiency (figure 3). To better understand the cause of this aminoacylation deficiency, we performed end-point pyrophosphate exchange experiments. At a phenylalanine concentration of 15 μM, twice the reported K_M for human mtPheRS, mutant P85A is unable to produce a measurable amount of activity, suggesting that the K_m of P85A for Phenylalanine is higher than the reported WT value. H135D mtPheRS showed a moderate amount of activity, suggesting that the observed aminoacylation deficiency is likely due to a defect in tRNA binding and not amino acid activation (figure 3).

The stability of WT and mutant proteins was assessed by active site titration after incubation at either room temperature or 37 °C. At room temperature, neither mutation has a measurable impact on protein stability. However, when tested at 37 °C, mutant P85A appears to have decreased stability when compared to WT (figure 3a, 3b).

Clinical Phenotype

The patient was the second child of healthy, non-consanguineous parents born without complication at 38 weeks gestation via normal spontaneous vaginal delivery. The pregnancy was complicated by gestational diabetes; the perinatal period was unremarkable. She was noted to have no major dysmorphic features. As an infant she was noted to have both motor and speech delays, first walking independently at 17 months, running at 24 months, and requiring a gait belt for safe ambulation at 5 years of age. Fine motor delays were likewise noted through school age. She spoke her first word at age 3.5 years. Her parents reported that her language skills plateaued at age 5-7 years at which point she was speaking in 3-4 word sentences with frequent grammatical errors. Paucity of speech and marked word retrieval difficulties were noted at age 9 years, at which time her neurologic exam revealed no focal findings beyond the aforementioned developmental delays.

Her first seizure, a prolonged generalized tonic-clonic convulsion, occurred at 8 years of age at which time antiepileptic therapy was initiated. Electroencephalogram (EEG) at age 9 years revealed mild background slowing in full wakefulness, as well as frequent epileptiform discharges without clinical correlate, including 3.0-3.5 Hertz (Hz) spike and slow wave discharges with bifrontal predominance, frequent runs of semi-rhythmic generalized 3 Hz slowing maximal over the left frontal region, and frequent runs of irregular sharp-slow wave activity, predominantly occurring over the right posterior quadrant. These discharges increased in frequency with sleep, occupying 65-70% of her sleep record. This initially responded to high-dose (1 mg/kg) diazepam with significant improvement of her EEG and some improvement in her speech and motor skills. Her EEG, however, again worsened with increasingly frequent bursts of generalized 3-4 Hz spike and wave activity in wakefulness and increasingly frequent generalized spikes in sleep. Her epilepsy both evolved and progressed, despite management with multiple antiepileptic medications (including valproate, with no resultant liver dysfunction) with focal seizures and epilepsia partialis continua occurring with increased frequency starting at 10 years of age. At age 13, she developed status epilepticus and progressed to have multiple subsequent events of status epilepticus that proved refractory to standard medical management, two experimental

medical trials, the ketogenic diet, and corpus callostomy. This progression of her epilepsy was accompanied by the development and progressive worsening of non-epileptic myoclonus. Notably, the corpus callostomy was complicated by subdural fluid collection requiring external ventricular drain placement. MRI brain at that time revealed extensive areas of abnormal T2 hyperintensity in the frontal lobes (right greater than left), anterior cingulate gyri, left superior frontal gyrus, bilateral temporal lobes, and left cerebellar cortex in the setting of recent seizure. MR spectroscopy in the left basal ganglia region demonstrated an unremarkable metabolic spectrum. Repeat multi voxel MR spectroscopy of the bilateral cerebral hemispheres one year later also showed normal metabolite ratios.

Despite a notable absence of disease process in any other organ or system, her neurologic status progressively deteriorated throughout this time. She had a mild decline in skills from ages 9-10 after an initial improvement following diazepam administration, and further decline with her convulsive seizures beginning at age 10. The patient's neurological status precipitously declined after the onset of her initial episode of status epilepticus at age 13 and, 10 days prior to death at the age of 15 years, her neurologic exam was notable for inability follow commands or track faces, bilaterally unreactive pupils, near-continuous myoclonus of the right face, arm, and leg, absence of purposeful movement, and up-going toes bilaterally. Repeat MRI brain performed 2 months prior to death demonstrated the presence of the known fluid collection as well as T2 hyperintensity within the left caudate and left medial temporal lobe, and the right medial occipital lobe along the superior bank of the right calcarine sulcus with encephalomalacia of the calcaravis (figure 4). EEG performed weeks prior to death revealed generalized, irregular theta and delta background slowing and near-continuous bi-hemispheric independent and synchronous epileptiform discharges over the fronto-temporal regions with shifting side predominance, at times corresponding to myoclonus, but more often not synchronous with the clinical myoclonus. She was hospitalized with likely pneumonia and urinary tract infections and died after being found apneic with pulseless arrest. An autopsy was performed.

Enzymatic, histological, and autopsy findings

Skeletal muscle biopsy was obtained at age 14 years and notable for predominantly type 2 fiber atrophy with rounded, atrophic fibers scattered throughout with rare regenerative fibers but without type grouping on H&E, ATPase PH 4.3, 4.6, and 9.4 stains. There was no evidence of inflammation or myonecrosis. NADH staining showed targetoid fibers. Gomoritrichome, PAS, and oil red O stains demonstrated normal patterns of staining. Combined COX/SDH stain was unremarkable. Electron microscopy revealed fibers with focal myofibrillary disarray, many myelin figures, abundant enlarged and swollen mitochondria containing glycogen and no inclusions (supplemental figure 1).

Polargraphic analysis of oxidative phosphorylation performed at the Center for Inherited Disorders of Energy Metabolism (CIDEM, Case Western Reserve University) demonstrated normal activity of Complexes I-IV (frozen specimen). Mitochondrial DNA content of skeletal muscle (qPCR analysis, performed at Baylor University) was reported at 61% of control (within normal). Normal pyruvate dehydrogenase, pyruvate carboxylase activity was noted in skin fibroblasts. “Markedly decreased” butyrobetaine, suggestive of a defect in

carnitine biosynthesis was noted in the same specimen but these findings are likely attributable to the patient's therapeutic ketogenic diet.

Autopsy gross specimens revealed a normal sized heart, enlarged liver (1960gm, normal 1500-1800gm), superficial hemorrhagic necrosis of the colon, and a small brain (830g, normal 1250-1400 g; 1.4% TBW). Microscopic analysis of brain and spinal cord revealed a diffuse, predominantly cortical, as well as subcortical process characterized by laminar cortical neuron loss and gliosis, diminished subcortical white matter and descending corticospinal tracts. The most severely affected regions included the bilateral frontoribital cortices and the bilateral primary visual cortices. In frontorbital cortex there was almost complete absence of neurons, excessive gliosis, pale white matter, and fragmenting of the cortical layers. The primary visual cortex is notable for a devastated line of Genari, almost complete absence of neurons, excessive gliosis, pale white matter, and fragmenting of the cortical layers extending through cortical layer 5. Notably, a large autopsy series of 32 patients with Alpers-Huttenlocher syndrome (a progressive degenerative encephalopathy related to polymerase gamma mutations) has previously reported characteristic findings of macroscopic cortical thinning, microscopic spongiosis with neuronal loss and astrocytosis that is most severe in the occipital lobe[17, 18]. Similar findings were also reported in an infant with *FARS2* mutations and progressive myoclonus epilepsy[10]. Additionally, a small region of spongiform change was noted in the right thalamus (figure 5) which was reminiscent of the spongiform lesions with relative neuronal sparing that have been reported in the basal ganglia of patients with Leigh syndrome bilaterally[19], though this finding was notably unilateral.

Discussion

Here, we report a case of compound heterozygous *FARS2* mutations in association with childhood onset refractory epilepsy, progressive myoclonus, cortical necrosis similar that seen on autopsy in Alpers-Huttenlocher syndrome as well as a previously reported case of *FARS2* mutation-associated infantile onset disease, and limited basal ganglia spongiform findings similar to those observed in Leigh syndrome. We additionally present bioinformatics and biochemical data to support a causal link. The clinical course, neuroimaging, and neuropathological findings[10] we report are strikingly similar to cases described in association with distinct *FARS2* mutations in two previous publications[10, 11], with the exception of age of onset, supporting a genetic association while suggesting an attenuated phenotype in this case. Together, these data support a distinct neuropathologic process related to perturbations of mtPheRS function. This report underscores the phenotypic variability associated with *FARS2* mutations and highlights the utility of genetic testing in cases of severe, refractory epilepsy and developmental delay.

The data presented here provides a plausible explanation for pathogenicity of the *FARS2* mutations observed. Taken together, the kinetic assays support a deficiency in the activation of amino acid for P85A, and a deficiency in the transfer of activated amino acid to tRNA for H135D mtPheRS. Additionally, P85A mtPheRS proteins demonstrated decreased stability at body temperature.

Because proline-85 is buried and surrounded by 5 aromatic residues within a 5Å radius (histidine-48, tyrosine-288, phenylalanine-296, phenylalanine-303, and phenylalanine-307), it is conceivable that perturbation of this residue might impact the stability of tertiary structural elements. Regarding the H135D substitution, review of the $tRNA^{Phe}$ bound *T. thermophilus* PheRS structure reveals that the sidechain hydroxyl group of tyronsine-267 lies within 3.5Å of a histidine-135 nitrogen, creating the possibility of a weak electrostatic interaction that might influence the tertiary structure of two loops that surround the acceptor stem of the tRNA. Disruption of such an interaction by charge reversal at the 135 position could potentially interfere with the binding of the acceptor stem, a possibility supported by experiments with recombinant mutant proteins. Presumably, these defects are each less potent than those observed in previously published cases.

Two features of interest are raised by this case. This case represents compound heterozygous mutations of a mt-aaRS, which has been seen in a preponderance of reports linking mt-aaRS mutations and clinical phenotypes, perhaps due to a frequently embryonic lethal homozygous phenotype in the case of most mt-aaRS mutations[1] Additionally, despite variation in severity of clinical presentation and duration of illness (presumably sufficient to impact other organ systems), the apparent nervous system-specificity of published phenotypes associated with *FARS2* perturbations is preserved. Similar tissue or organ system specificities have been noted with genetic perturbation of other mitochondrial mt-aaRS[2, 3, 4, 5, 6]. It remains to be determined whether this is a result of a relative but differential impact on the expression of specific mitochondrially encoded peptides or the crossing of a threshold of generalized organelle dysfunction to which a given tissue—particularly nervous system tissues—might be more sensitive. Further work is required to more precisely delineate the pathogenic mechanisms underlying mutations in mt-aaRS proteins as well as all diseases affecting mitochondrial translation.

Acknowledgments

Funding: Research Education Programs for Residents and Fellows in Neurology, Neurosurgery, Neuropathology and Neuroradiology (R25), (RFAs: NS-09-001, NS-10-002, NS-12-003) to M.A.W.

National Science Foundation MCB- 1412611 to M.I.

References

1. Konovalova S, Tyynismaa H. Mitochondrial aminoacyl-tRNA synthetases in human disease. Mol Genet Metabol. 2013; 108:206–211.
2. Hallmann K, Zsurka G, Moskau-Hartmann S, Kirschner J, Korinthenberg R, Ruppert AK, Ozdemir O, Weber Y, Becker F, Lerche H, Elger CE, Thiele H, Nürnberg P, Sander T, Kunz WS. A homozygous splice-site mutation in CARS2 is associated with progressive myoclonic epilepsy. Neurology. 2014; 83:2183–7. [PubMed: 25361775]
3. Scheper GC, van der Klok T, van Andel RJ, van Berkel CG, Sissler M, Smet J, Muravina TI, Serkov SV, Uziel G, Bugiani M, Schiffmann R, Krägeloh-Mann I, Smeitink JA, Florentz C, Van Coster R, Pronk JC, van der Knaap MS. Mitochondrial aspartyl-tRNA synthetase deficiency causes leukoencephalopathy with brain stem and spinal cord involvement and lactate elevation. Nat Genet. 2007; 39:534–9. [PubMed: 17384640]
4. Steenweg ME, Ghezzi D, Haack T, Abbink TE, Martinelli D, van Berkel CG, Bley A, Diogo L, Grillo E, Te Water Naudé J, Strom TM, Bertini E, Prokisch H, van der Knaap MS, Zeviani M.

Leukoencephalopathy with thalamus and brainstem involvement and high lactate 'LTBL' caused by EARS2 mutations. Brain. 2012; 135:1387–94. [PubMed: 22492562]

5. Bayat V, Thiffault I, Jaiswal M, Tétreault M, Donti T, Sasarman F, Bernard G, Demers-Lamarche J, Dicaire MJ, Mathieu J, Vanasse M, Bouchard JP, Rioux MF, Lourenco CM, Li Z, Haueter C, Shoubridge EA, Graham BH, Brais B, Bellen HJ. Mutations in the mitochondrial methionyl-tRNA synthetase cause a neurodegenerative phenotype in flies and a recessive ataxia (ARSAL) in humans. PLoS Biol. 2012; 10(3):e1001288. [PubMed: 22448145]
6. Edvardson S, Shaag A, Kolesnikova O, Gomori JM, Tarassov I, Einbinder T, Saada A, Elpeleg O. Deleterious mutation in the mitochondrial arginyl-transfer RNA synthetase gene is associated with pontocerebellar hypoplasia. Am J Hum Genet. 2007; 81:857–62. [PubMed: 17847012]
7. Rotig A. Human diseases with impaired mitochondrial protein synthesis. Biochim Biophys Acta. 2011; 1807:1198–1205. [PubMed: 21708121]
8. Brandon MC, Lott MT, Nguyen KC, Spolim S, Navathe SB, Baldi P, Wallace DC. MITOMAP: a human mitochondrial genome database--2004 update. Nucleic Acids Res. 2005 Jan 1; 33(Database issue):D611–3. [PubMed: 15608272]
9. Shamseldin HE, Alshammari M, Al-Sheddi T, Salih MA, Alkhalidi H, Kentab A, Repetto GM, Hashem M, Alkuraya FS. Genomic analysis of mitochondrial diseases in a consanguineous population reveals novel candidate disease genes. J Med Genet. 2012; 49:234–41. [PubMed: 22499341]
10. Elo JM, Yadavalli SS, Euro L, Isohanni P, Götz A, Carroll CJ, Valanne L, Alkuraya FS, Uusimaa J, Paetau A, Caruso EM, Pihko H, Ibba M, Tyynismaa H, Suomalainen A. Mitochondrial phenylalanyl-tRNA synthetase mutations underlie fatal infantile Alpers encephalopathy. Hum Mol Genet. 2012; 21:4521–9. [PubMed: 22833457]
11. Almalki A, Alston CL, Parker A, Simonic I, Mehta SG, He L, Reza M, Oliveira JM, Lightowlers RN, McFarland R, Taylor RW, Chrzanowska-Lightowlers ZM. Mutation of the human mitochondrial phenylalanine-tRNA synthetase causes infantile-onset epilepsy and cytochrome c oxidase deficiency. Biochim Biophys Acta. 2014; 1842:56–64. [PubMed: 24161539]
12. The PyMOL Molecular Graphics System, Version 1.8. Schrödinger, LLC;
13. Yadavalli SS, Klipcan L, Zozulya A, Banerjee R, Svergun D, Safro M, Ibba M. Large-scale movement of functional domains facilitates aminoacylation by human mitochondrial phenylalanyl-tRNA synthetase. FEBS Lett. 2009; 583:3204–3208. [PubMed: 19737557]
14. Kyte J, Doolittle R. A simple method for displaying the hydropathic character of a protein. J Mol Biol. 1982; 157:105–132. [PubMed: 7108955]
15. Klipcan L, Levin I, Kessler N, Moor N, Finarov I, Safro M. The tRNA-Induced Conformational Activation of Human Mitochondrial Phenylalanyl-tRNASynthetase. Structure. 2008; 16:1095–1104. [PubMed: 18611382]
16. Goldgur Y, Mosyak L, Reshetnikova L, Ankilova V, Lavrik O, Khodyreva S, Safro M. The crystal structure of phenylalanyl-tRNAsynthetase from thermusthermophilus complexed with cognate tRNAPhe. Structure. 1997; 5:59–68. [PubMed: 9016717]
17. Harding BN. Progressive Neuronal Degeneration of Childhood with Liver Disease (Aplers-Huttenlocher Syndrome): A Personal Review. J Child Neurol. 1990; 5:273–87. [PubMed: 2246481]
18. Naviaux RK, Nguyen KV. POLG mutations associated with Alpers' syndrome and mitochondrial DNA depletion. Ann Neurol. 2004; 55:706–12. [PubMed: 15122711]
19. M Gerards, M.; Sallevelt, SCEH.; Smeets, HJM. Leigh syndrome: Resolving the clinical and genetic heterogeneity paves the way for treatment options. Mol Genet Metab. 2015. http://dx.doi.org/10.1016/j.ymgme.2015.12.004

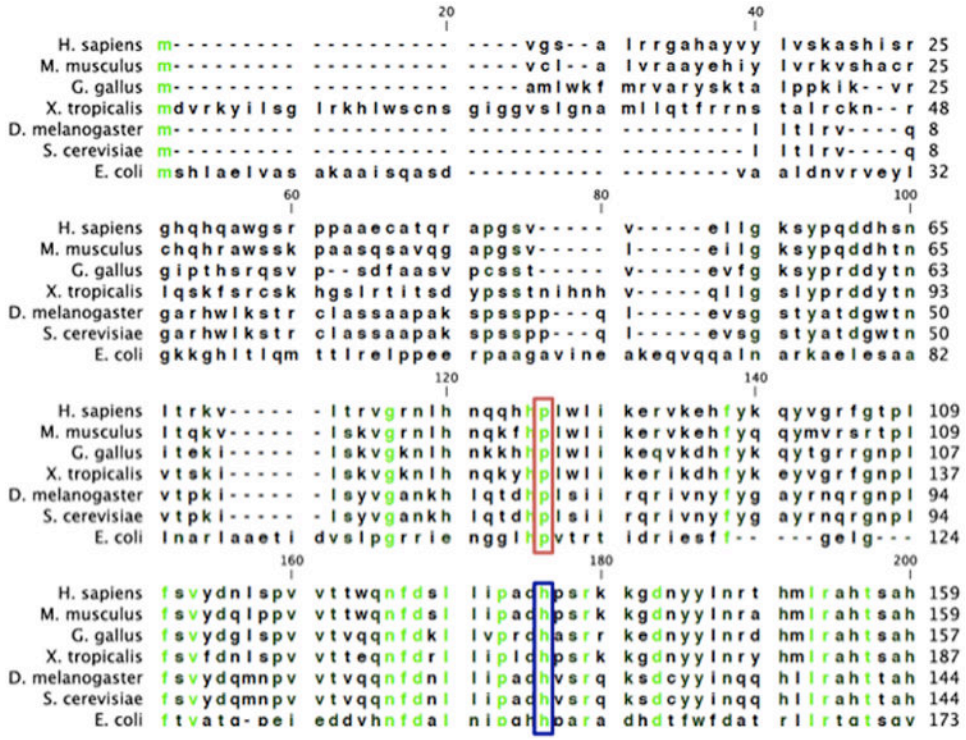

Figure 1. Multiple sequence alignment of orthologous proteins

Multiple sequence alignment of N-terminal mitochondrial phenylalanyl transfer RNA synthetase peptide sequences from multiple species. Conserved residues are presented in green. The location of the mutations carried by the patient are boxed in red (proline-85) and blue (histidine-135). Both residues are highly conserved through bacterial species.

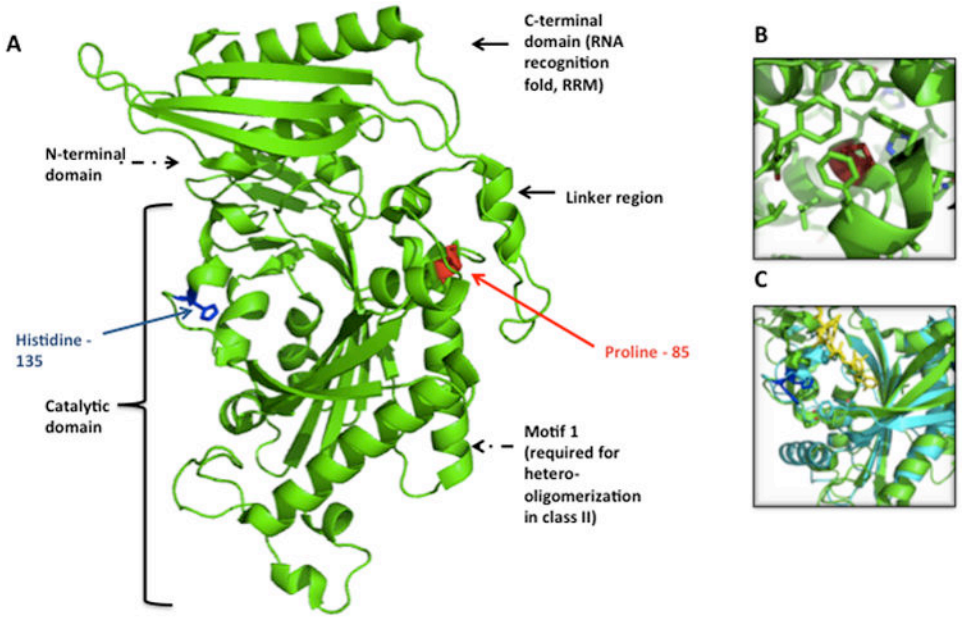

Figure 2. Structure-guided analysis of *FARS2* mutations

Structure-guided analysis of *FARS2* mutations. Phe-AMP bound *FARS2* quarternary structure with domains labeled (PBD id 3CMQ), the locations of proline-85 and histidine-135 are highlighted in red and blue, respectively (A). proline-85 is buried within several aromatic residues (B). histidine-135 is located within conserved inter-motif region forming one of two catalytic domain loops which associate with the acceptor stem of the tRNA molecule in the crystal structure of the orthologous protein T. Thermophilus-PheRS-bound to tRNA-Phe (PBD id 1EIY), pictured here in cyan with orthologous domain aligned with *FARS2* in green, tRNA-Phe is drawn in yellow.

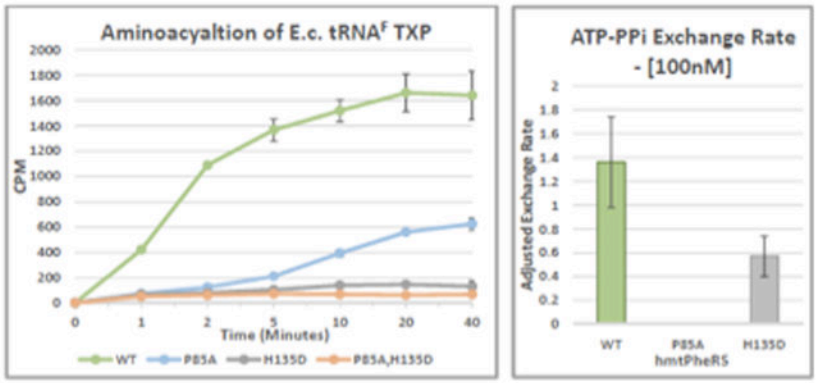

mtPheRS	K_{cat}^{tRNA} (s^{-1})	K_M^{tRNA} (μM)	K_{cat}/K_M (s^{-1} μM^{-1})
WT	0.16 ± 0.030	1.2 ± 0.04	0.14 ± 0.02
P85A	0.13 ± 0.008	0.4 ± 0.04	0.30 ± 0.04
H135D	*ND*	*ND*	*ND*

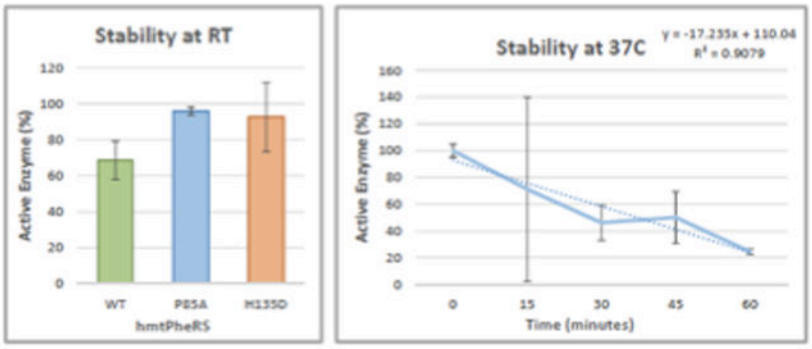

Figure 3. Analysis of recombinant mutant enzymes

Recombinant mutant mtPheRS proteins were expressed and purified in *E. coli* per established protocols. End point aminoacylation reactions indicated that mutant P85A mtPheRS charges tRNA very similarly to WT, but H135D demonstrated severe aminoacylation deficiency. Determination of the steady-state kinetics for tRNA revealed that mutant P85A has a two-fold increase in catalytic efficiency when compared to WT, while kinetic parameters for H135D were unable to be determined using standard techniques, reinforcing the previously observed aminoacylation deficiency. End-point pyrophosphate exchange experiments were also performed. At a phenylalanine concentration of 15 μM, twice the reported Km for human mtPheRS, mutant P85A is unable to produce a measurable amount of activity, suggesting that the Km of P85A for phenylalanine is higher than the reported WT value. Mutant H135D mtPheRS showed a moderate amount of activity, suggesting that the observed aminoacylation deficiency is likely due to a defect in tRNA binding and not amino acid activation. The stability of WT and mutant proteins was assessed by active site titration after incubation at either room temperature or 37 °C. At room temperature, neither mutation has a measurable impact on protein stability. However, when tested at 37 °C, mutant P85A appears to have decreased stability when compared to WT.

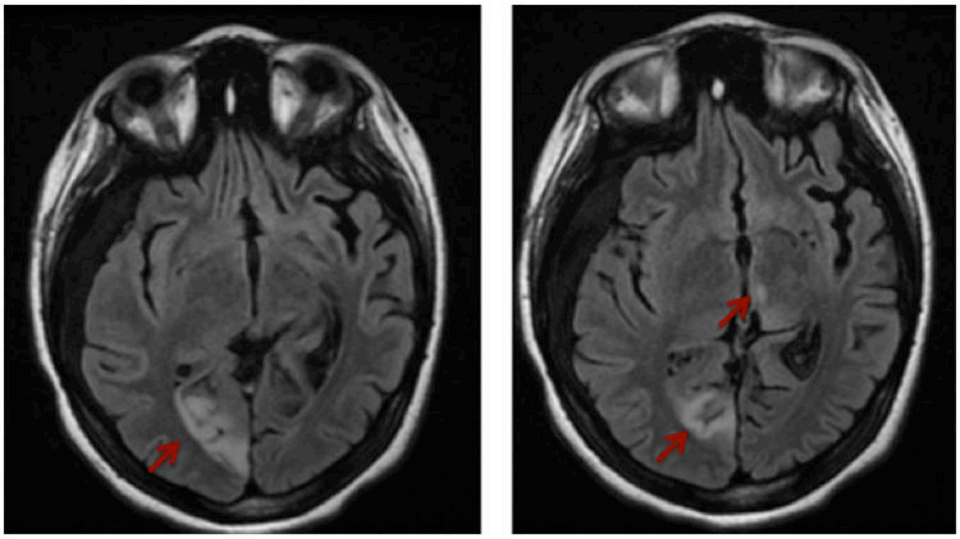

Figure 4. MRI brain

MRI brain performed at age 15 years, 2 months prior to death revealing T2 hyperintensity within the left caudate and left medial temporal lobe, and the right medial occipital lobe along the superior bank of the right calcarine sulcus with encephalomalacia of the calcaravis. Notably, earlier corpus callostomy for refractory seizures was complicated by the right subdural fluid collection also seen in this image, requiring external ventricular drain placement.

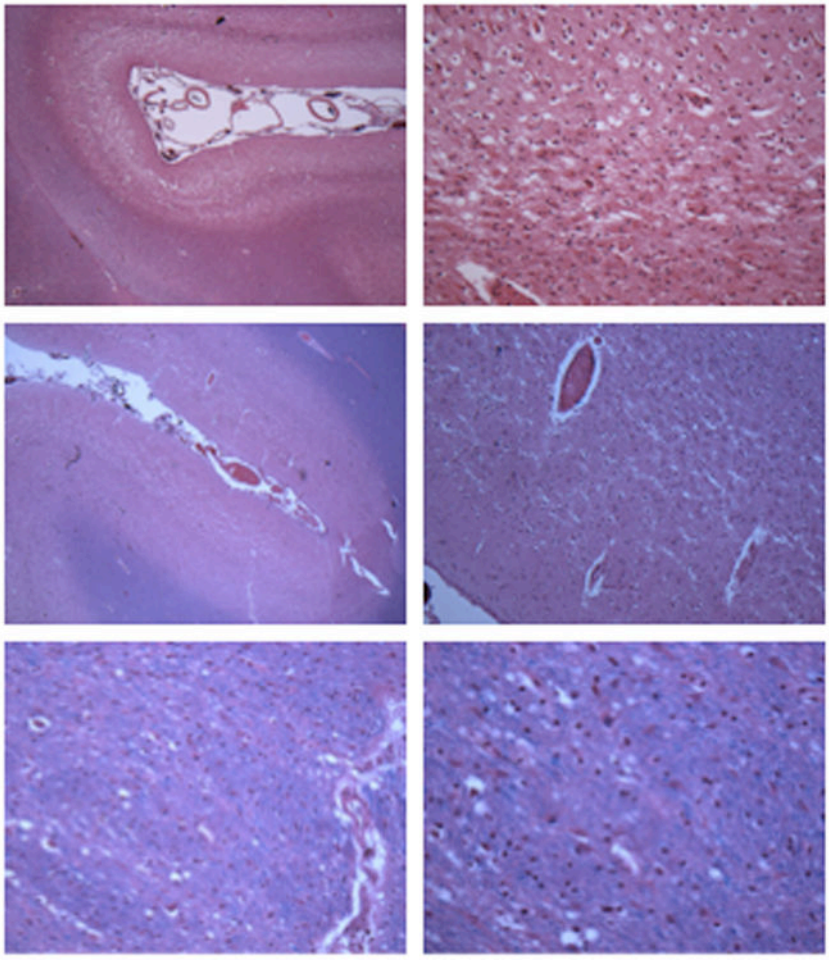

Figure 5. Microscopic analysis of brain and spinal cord on autopsy

Microscopic analysis of the brain and spinal cord revealed a diffuse, predominantly cortical, as well as subcortical process characterized by laminar cortical neuron loss and gliosis, with the the primary visualcortex, seen in low (A) and high (B) power, and the lateral occipital cortex, seen in low (C) and high (D) power markedly affected. A single focal region of spongiform change was observed in the thalamus, shown at low (E) and high (F) power.

Table 1

Summary of Reported Cases with *FARS2* Perturbations

Summary of clinical, laboratory, and experimental findings associated with the 6 reported cases in the English literature of patients with likely pathologic *FARS2* mutations. Abbreviations: ragged red fibers (RRF)

Citation	Age, Gender	Genetic findings	Clinical phenotype	MRI	Enzyme Activity	Muscle Histology	Lactate	Neuropathology	Functional Assay
Al Malki et al	6 mo. male, (living at publication)	D325Y, deletion	myoclonus, epilepsy, developmental delay	white matter abnormalities	decreased COX	decreased COX staining			
Elo et al	8 mo. female, (deceased)	I329T, D391F cmpd het in trans	myoclonus, epilepsy, developmental delay	cortical atrophy, increased putaminal signal	decreased COX, SDH	Glycogen accumulation, no RRF	Increased in serum, CSF, lactate peak on MRS	brain wgt <30% of nml, generalized atrophy, gliosis subtotal laminar necrosis of the cortical ribbon	*in vitro* aminoacylation activity; refolding
Elo et al	21 mo. female, (deceased)	sister of #2	myoclonus, epilepsy, developmental delay				Increased (specimen type not reported)		
Shamseldin et al	22 mo., (deceased)	homozygous Y144C	myoclonus, epilepsy, developmental delay	cortical atrophy, increased putaminal signal, subdural fluid accumulation		no RRF	Increased serum		*in vitro* aminoacylation activity; refolding
Shamseldin et al	3 mo., (deceased)	homozygous Y144C	myoclonus, epilepsy, developmental delay						
Shamseldin et al	3 mo., (deceased)	homozygous Y144C	myoclonus, epilepsy, developmental delay						

*Blank fields were not reported in corresponding publications.

Table 2

Summary of Pathologic Findings

Summary of autopsy brain histology features found in the case presented, a previously published case of infantile onset *FARS2* mutation associated disease, Alpers-Huttenlocher Syndrome, and Leigh Syndrome

	Case presented	**Infantile onset *FARS2* case (Elo et al., 2012)**	**Alpers-Huttenlocher Syndrome (Harding, 1990)**	**Leigh Syndrome (Gerards et al., 2015)**
Microscopic Findings	Finding 1. Almost complete absence of neurons, excessive gliosis, pale white matter, and fragmenting of the cortical layers. Finding 2. Spongiform change	Finding 1. "Striking and subtotal laminar necrosis of the whole cortical ribbon. Degeneration … was almost total, with … mid-laminar microcystic degeneration with reactive gliosis and capillary proliferation…" Finding 2. "Neuronal degeneration with atrophy and gliosis …." Finding 3. "Severely atrophic with Purkinje cell drop-out, narrowed molecular and granular layers"	"Laminar dehiscence … mild superficial astrocytosis through increasing sponginess, nerve cell loss, and gliosis, until the whole ribbon is thinned and depleted of nerve cells and the neuropil is disorganized and replaced by hypertrophic fiber-forming astrocytes and a prominent vascularity."	"Microscopically, they have a spongiform appearance due to hypervascularity with capillary proliferation and endothelial swelling, and they are associated with gliosis and demyelination, with relative sparing of neurons."
Region of greatest severity	Finding 1. Occipital cortex, frontal cortex Finding 2. Right thalamus	Finding 1. Frontal cortex Finding 2. Basal ganglia Finding 3. Cerebellar cortex	Calcarine cortex	Basal ganglia, thalamus, brain stem, cerebellum, optic nerves, & spinal cord